

WKS-type distributionally robust optimisation for optimal sub-hourly look-ahead economic dispatch

ISSN 1751-8644
 doi: 0000000000
www.ietdl.org

Yang Liu¹, Xianbang Chen¹, Bin Li¹, Huaqiang Li^{1*}, Yanli Ye¹

¹ College of Electrical Engineering, Sichuan University, Chengdu, China

* E-mail: lihuaqiang@scu.edu.cn

Abstract: Renewable energy sources, particularly wind power, are being increasingly deployed in power systems to reduce environmental contamination. However, the uncertainty of wind power significantly influences power system economy. Therefore, this paper presents Wiesemann–Kuhn–Sim (WKS)-type distributionally robust optimisation for performing an optimal two-stage sub-hourly look-ahead economic dispatch considering uncertain wind power. The dispatch considers the scheduling of thermal generators, wind power generators, and fast-response resources. The optimisation aims at minimising the expected total operational cost, including the costs of generation, generation shedding, and wind power curtailment. The hourly stage determines the thermal generation that can withstand the worst-case wind power distribution. The sub-hourly stage schedules the fast-response operations to correct the hourly dispatch. To characterise the uncertainty, a novel WKS-format ambiguity set that can obtain wind power distribution from historical data is constructed using the lifting theorem. Based on the ambiguity set and linear decision rule, a general lemma is employed to convert the model into a tractable conic optimisation that can be directly solved. Experimental results demonstrate the effectiveness of the presented approach compared to adjustable robust optimisation and sample-based stochastic optimisation.

Nomenclature

Indices and sets

i/\mathcal{N}_g	Index/set of thermal generators.
v/\mathcal{N}_y	Index/set of decisions of sub-hourly RED. \mathcal{N}_y is equal to the dimension of \mathbf{y}^s .
q/\mathcal{N}_l	Index/set of loads.
t/\mathcal{N}_t	Index/set of transmission lines.
j/\mathcal{N}_w	Index/set of wind farms.
d/\mathcal{N}_d	Index/set of sub-hourly RED.
s/\mathcal{N}_s	Index/set of stochastic variables \tilde{w}_s , \mathcal{N}_s = \mathcal{N}_w \times \mathcal{N}_d .
\mathcal{N}	Number of elements in set \mathcal{N} .

Look-ahead economic dispatch variables

\mathbf{p}	Vector of LED decisions.
p_i	Output of generator i .
\mathcal{X}	Feasible set of LED.

Look-ahead economic dispatch parameter

p_i^0	Generation of generator i in last LED.
p_i^{min}/p_i^{max}	Minimal/maximal output of generator i .
R_i^{up}/R_i^{dn}	Ramp-up/ramp-down capacity of generator i .
a_i, b_i	Production cost coefficients of generator i .
Γ	Budget parameter of A-SLED.

Sub-hourly real-time economic dispatch variables

\mathbf{y}	Vector of sub-hourly RED decisions, $\mathbf{y} = \{\mathbf{w}^c, \mathbf{l}^s, \mathbf{p}^s, \mathbf{r}^+, \mathbf{r}^-\}$.
--------------	--

$\tilde{\mathbf{w}}$	Vector of stochastic wind power generation.
\tilde{w}_{dj}	Stochastic wind power generation of wind farm j in sub-hourly RED d .
\mathbf{w}^c	Vector of $w_{dj}^c, \forall d \in \mathcal{N}_d, \forall j \in \mathcal{N}_w$.
w_{dj}^c	Curtailment of wind farm j in sub-hourly RED d .
\mathbf{l}^s	Vector of $l_{dq}^s, \forall d \in \mathcal{N}_d, \forall q \in \mathcal{N}_l$.
l_{dq}^s	Shedding of load q in sub-hourly RED d .
\mathbf{p}^s	Vector of $p_{di}^s, \forall d \in \mathcal{N}_d, \forall i \in \mathcal{N}_g$.
p_{di}^s	Generation shedding of generator i in sub-hourly RED d .
r^+/r^-	Vector of $r_{di}^+/r_{di}^-, \forall d \in \mathcal{N}_d, \forall i \in \mathcal{N}_g$.
r_{di}^+/r_{di}^-	Ramp-up/ramp-down fast-response resource i in sub-hourly RED d .

Sub-hourly real-time economic dispatch parameters

c_{dj}^w	Cost coefficient of curtailment of wind farm j in sub-hourly RED d .
c_{dq}^l	Cost coefficient of shedding of load q in sub-hourly RED d .
c_{di}^g	Cost coefficient of shedding of generator i in sub-hourly RED d .
l_{dq}	Demand of load q in sub-hourly RED d .
F_t	Power flow capacity of transmission line t .
τ_{it}	Power transfer distribution factor of line t from generator i .
τ_{jt}	Power transfer distribution factor of line t from wind farm j .

τ_{qt}	Power transfer distribution factor of line t from load q .	WPG	Wind power generator.
r_{di}^{up}/r_{di}^{dn}	Ramp-up/ramp-down capacity of fast-response resource i in sub-hourly RED d .	DC	Direct current.
<i>Parameters of ambiguity sets</i>		UC	Unit commitment.
d	Coefficient matrix of sub-hourly RED objective in compact formulation.	ED	Economic dispatch.
T	Coefficient matrix of p in compact formulation.	DED	Day-ahead economic dispatch.
W	Coefficient matrix of y in compact formulation.	LED	Look-ahead economic dispatch.
b	Coefficient matrix in compact formulation.	RED	Real-time economic dispatch.
w^{min}/w^{max}	Vector of w_s^{min}/w_s^{max} .	AGC	Automatic generation control.
w_s^{min}/w_s^{max}	Minimal/maximal value of \tilde{w}_s .	SLED	Sub-hourly resolution LED.
μ	Vector of μ_s .	HLED	Hourly resolution LED.
μ_s	First-order value of \tilde{w}_s .	DO	Deterministic optimisation.
σ	Vector of σ_s .	SO	Stochastic optimisation.
σ_s	Second-order value of \tilde{w}_s .	ARO	Adjustable robust optimisation.
ξ	Vector of ξ_s .	DRO	Distributionally robust optimisation.
ξ_s	Third-order value of \tilde{w}_s .	PDF	Probability distribution function.
$E_{ \mathcal{N} }$	$ \mathcal{N} $ -dimension identity matrix.	WKS	Wiesemann–Kuhn–Sim.
<i>Variables of ambiguity sets</i>		D-SLED	Distributionally robust sub-hourly LED.
$y(\tilde{w})$	Decision rule as affine function of \tilde{w} .	D-HLED	Distributionally robust hourly LED.
y^s	Decision vector related to \tilde{w}_s .	S-SLED	Stochastic sub-hourly LED.
y_v^s	Element v of y^s .	A-SLED	Adjustable robust sub-hourly LED.
\tilde{w}_s	Stochastic wind power generation s .	MCS	Monte Carlo simulation.
\tilde{u}	Vector of auxiliary variable introduced into the WKS-format set.	LP	Linear program.
\tilde{u}_s	Element s of \tilde{u} .		
$\alpha, \beta, \varphi, L$	Dual variables.		
<i>Sets and functions</i>			
Ω	Support set.		
\mathcal{K}	Regular cone.		
\mathcal{K}^*	Dual cone of \mathcal{K} .		
$\mathbb{L}^{ \mathcal{N} }$	$ \mathcal{N} $ -dimension second-order cone.		
$\mathbb{R}^{ \mathcal{N}_g \times \mathcal{N}_y }$	$\mathbb{R}^{ \mathcal{N}_g } \times \mathbb{R}^{ \mathcal{N}_y }$ real space.		
$\mathbb{R}_+^{ \mathcal{N} }$	$ \mathcal{N} $ -dimension non-negative real space.		
\mathbb{P}	Distribution of \tilde{w} .		
$c(x)$	Cost function of LED strategy x .		
$Q(x, \tilde{w})$	Cost function of RED strategy y based on x and \tilde{w} .		
$\Pi_{\tilde{w}} \mathcal{P}$	Marginal distribution of \tilde{w} over \mathcal{P} .		
$\ \cdot\ _2$	2-norm of a vector.		
$\mathbb{E}_{\mathbb{P}}[\cdot]$	Expectation over distribution \mathbb{P} .		
$\mathcal{P}(\mathbb{R}^{ \mathcal{N}_s } \times \mathbb{R}^{ \mathcal{N}_s })$	Space of probability distribution on $\mathbb{R}^{ \mathcal{N}_s } \times \mathbb{R}^{ \mathcal{N}_s }$.		
$\mathbb{P}[\cdot]$	Probability of an event.		
<i>Abbreviations</i>			
IER	Intermittent energy resource.		

1 Introduction

Currently, several conventional power sources, such as coal power, are used in power systems. This results in severe environmental contamination [1]. Therefore, renewable energy sources, particularly intermittent energy resources (IERS), have been widely deployed in power systems to reduce environmental contamination [2]. However, because of the uncertainties of IERS, particularly wind power, it is difficult to balance load demand moment-by-moment on the generation side without violating the operational constraints of transmission networks. As a result, the imbalance may lead to frequent load shedding and high usage of reserve resources, which considerably affect power system economy [3, 4]. In this regard, studies [5-7] have focused on developing approaches to improve power system economy; among these, economic dispatch (ED) is considered one of the most effective methods [8-13].

To improve power system economy, ED divides a dispatch process into four sub-processes (day-ahead ED (DED), look-ahead ED (LED), real-time ED (RED), and automatic generation control (AGC) [8]) in order to increase the accuracy of the dispatch strategy. During the ED process, DED [28] provides results pertaining to unit commitment (UC), the level of fast-response resources, and the base generation of thermal generators in the day-ahead stage; LED [25] corrects the base generation of DED in the intra-day stage. On the basis of the revised base generation, RED [16] schedules the fast-response resources to handle minute-to-minute fluctuations while AGC [8] operates automatic units to cope with second-to-second fluctuations. Among these processes, LED is commonly considered to be an important underlying stage of ED [9-13] as it is the link between the day-ahead and intra-day stages. As a result, LED modelling improvements and advanced optimisation approaches have attracted considerable interest from researchers developing optimal LED plans including uncertain wind power.

Hetzer *et al.* [9] presented a single-stage LED model that assumed that wind speed follows the Weibull distribution. The authors converted the model to a chance-constrained model [10] and claimed

that the model is effective for achieving the optimal LED for a power system with uncertain wind power. Certain studies [11-13] employed single-stage models to optimise dispatch plans considering the uncertainty of IERs, thus validating the models. However, single-stage models cannot consider the prediction errors that occur when IER information is updated. As a result, two-stage LED models, which contain an additional second stage for simulating RED, have been widely developed to improve the accuracy of LED optimisation. Certain studies [14, 15] validated two-stage LED models at hourly resolution. However, other works [11, 16, 17] indicated that hourly-resolution LED (HLED) models neglect the sub-hourly fluctuations in wind power, which may result in operational insecurity. In this regard, a study [18] investigated the effects of IER fluctuations on power system operation at different resolutions. Experimental results demonstrated that sub-hourly resolution LED (SLED) models can effectively handle the sub-hourly fluctuations of IER by preventing energy imbalance, network congestion, and load loss issues.

Moreover, several works adopted heuristic algorithms, such as genetic algorithms [19], simulated annealing [20], and particle swarm optimisation [21], to solve LED models accurately and efficiently. However, it is widely known that these algorithms frequently experience locally optimal and premature issues [22]. Therefore, mathematical programming approaches have been investigated, particularly deterministic optimisation (DO), stochastic optimisation (SO), and adjustable robust optimisation (ARO). For example, studies [23, 24] employed DO for optimising ED and UC. However, Wu *et al.* [12] indicated that the feasibility of DO-based operational plans cannot be ensured because the uncertainty of IERs is neglected. Based on a predefined probability distribution function (PDF), SO [25, 26] generates numerous samples to represent uncertainty. Theoretically, the feasibility of optimisation considering uncertainty can be improved. However, the issues of computational intensiveness, over-optimism, and inaccurate PDFs prevent SO from being widely used. In this regard, ARO employs the worst-case scenario in an uncertainty set to implement easy-to-solve and secure uncertainty modelling [8, 27]. However, ARO may lead to over-conservativeness because only the worst-case scenario is considered [42].

Distributionally robust optimisation (DRO) [29] has remarkable optimisation ability because of its excellent uncertainty modelling ability based on utilising the statistical information obtained from historical data. DRO innovatively employs an ambiguity set to obtain the distributions of uncertainty using partial statistical information instead of the pre-assumed PDFs or simple sets. Hence, DRO can balance optimism and conservativeness. Based on ambiguity sets comprising mean and quadratic information, Wei *et al.* presented second-order moment DRO models for joint LED of energy and reserve dispatch [14] and RED [30] considering uncertain wind power. The authors applied decomposition and iteration algorithms to solve the models and further indicated that DRO can bridge the gap between SO and ARO in terms of economy, robustness, and computational efficiency. However, researches [15, 28] pointed out that the unbounded ambiguity sets in [14, 30] may involve unreasonably conservative distributions. Therefore, the authors further introduced interval information into the ambiguity sets, and then constructed less conservative DRO models for co-dispatch of hydro-thermal-wind power [15] and contingency-constrained UC [28]. Solving the models with constraint generation iteration algorithm [15] and the Benders decomposition approach [28], the authors demonstrated that these bounded ambiguity sets achieve better economy.

However, these applications [14, 15, 28, 30] of DRO to power systems are based on various complex decomposition methods and iteration algorithms that are challenging to extend and re-realisation. In this regard, Wiesemann, Kuhn, and Sim (WKS) [32] presented a general WKS-format ambiguity set that can be described by unified bounded conic constraints. Using the WKS-format ambiguity set, Li *et al.* [33] presented a WKS-type DRO, in which the complex reformulation of intractable two-stage DRO models into tractable models can be conveniently achieved by using a general theorem. Moreover, WKS-type DRO can flexibly employ information of various orders obtained from historical data while maintaining high

efficiency. As a result, WKS-type DRO significantly extends the previous work [32] into a class of two-stage SO problems, thus providing an excellent alternative for solving two-stage power system optimisation problems considering IER uncertainty.

Therefore, motivated by the aforementioned works, this paper presents a WKS-type DRO approach for optimising SLED for transmission networks considering uncertain wind power. The main works of this paper are as follows:

(1) A distributionally robust two-stage SLED model (D-SLED) is presented in this paper. D-SLED aims to minimize the expected total operational cost. The hourly first stage determines the LED strategy according to the worst-case wind power distribution while the sub-hourly second stage schedules fast-response operations. As a result, D-SLED effectively provides a robust and economic LED strategy.

(2) To capture wind power uncertainty, the *lifting theorem* [32] is applied to construct the WKS-format ambiguity set that contains interval, mean, quadratic, cubic, and even higher-order information instead of solely mean and quadratic information [14, 30]. Ultimately, the wind power uncertainty can be characterised accurately so that a less conservative LED can be achieved.

(3) Based on the linear decision rule [31, 34] and WKS-format ambiguity set, we employ a highly general theorem in [33] as a lemma to directly convert D-SLED into a tractable conic optimisation problem that can effectively be solved. Compared with previous DRO approaches based on constraint generation iteration methods [14, 15, 30, 42] or decomposition algorithms [28, 43], WKS-type DRO is more convenient and tractable to implement owing to the general theorem. Finally, the effectiveness of D-SLED is compared with that of DRO-based HLED (D-HLED), SO-based SLED (S-SLED), and ARO-based SLED (A-SLED) on the IEEE 118-bus transmission network.

The remainder of the paper is organised as follows: Section 2 presents the mathematical model of D-SLED. The details of the WKS-format ambiguity set and the equivalent conic reformulation of D-SLED are provided in Section 3. Section 4 presents and discusses the experimental results. Section 5 concludes the paper.

2 D-SLED modelling

2.1 Problem statement

Fig. 1 shows the four stages of a typical ED process. As uncertain wind power cannot be predicted accurately in the day-ahead stage, the inaccuracy issue generally results in uneconomic DED [11]. Therefore, economic operation strongly relies on the intra-day LED to correct the base generation of DED. Moreover, RED and AGC cannot handle the strong short-term fluctuations in wind power. Hence, these two intra-day stages must be implemented based on the revised set points of the generators; otherwise, load shedding will occur frequently [38, 39]. In this regard, the deployment of LED considerably eases the operational burdens on RED and AGC, thus improving operational feasibility and robustness [12, 13]. As a result, LED has been widely regarded as the key link between the day-ahead and intra-day stages.

Fig. 2 shows that conventional HLED only considers average wind power information across the dispatch horizon. However, SLED considers sub-hourly information by employing several sub-hourly RED processes for further improving operation economy. As a result, this paper focuses on D-SLED in order to provide an economic LED plan involving uncertain wind power.

2.2 Basic model of D-SLED

Although LED is commonly carried out every 15 min throughout the dispatch day, this paper presents a model representing only a single LED process among dynamic LED processes for a general and simplified analysis. In the presented model, UC results and capacities of fast-response resources have been determined in DED; wind power information and certain load demand forecasts are locked in

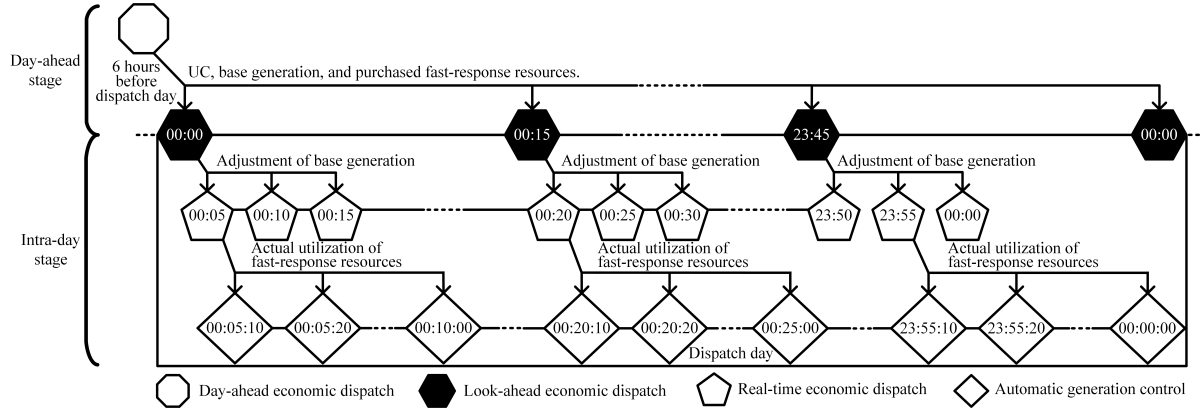


Fig. 1: Cooperation of DED, LED, RED, and AGC.

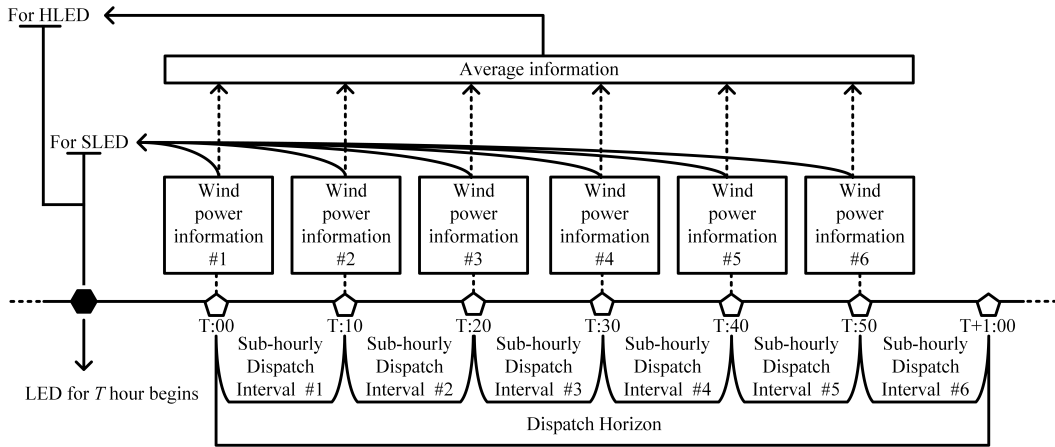


Fig. 2: Comparison of HLED and 10-min resolution SLED.

minutes before implementing LED optimisation. The initial generation of each generator is determined according to the previous LED strategy.

In the proposed two-stage D-SLED modelling, the first stage is to simulate LED, which determines the optimal LED strategy \mathbf{p} for available thermal generators before the observation of $\tilde{\mathbf{w}}$. The objective and constraints are represented as (1)–(3).

$$\min_{\mathbf{p}} \left\{ \sum_{i \in \mathcal{N}_g} [a_i(p_i)^2 + b_i p_i] + \sup_{\mathbb{P} \in \mathcal{P}} \mathbb{E}_{\mathbb{P}}[Q(\mathbf{p}, \tilde{\mathbf{w}})] \right\} \quad (1)$$

$$s.t. \quad p_i^{\min} \leq p_i \leq p_i^{\max}, \forall i \in \mathcal{N}_g, \quad (2)$$

$$R_i^{dn} \leq p_i - p_i^0 \leq R_i^{up}, \forall i \in \mathcal{N}_g. \quad (3)$$

In the dispatch horizon, constraints (2) and (3) indicate the generation limitation and ramping limitation, respectively. Considering that the worst wind power distribution \mathbb{P} of an ambiguity set \mathcal{P} will occur in RED, objective (1) aims at minimising the expected total operational cost.

As the thermal generation strategy is determined without observing $\tilde{\mathbf{w}}$, the plan may result in energy imbalance. Therefore, the second stage ((4)–(11)) is applied as the corrective action after realizing $\tilde{\mathbf{w}}$. This stage determines the optimal fast-response operations $\mathbf{y} = \{w^c, l^s, p^s, r^+, r^-\}$ in the sub-hourly RED processes. The operations comprise wind power curtailment w^c , load shedding l^s , generation shedding p^s , and the utilisation of fast-response resources r^+/r^- .

$$\sup_{\mathbb{P} \in \mathcal{P}} \mathbb{E}_{\mathbb{P}}[Q(\mathbf{p}, \tilde{\mathbf{w}})] = \sup_{\mathbb{P} \in \mathcal{P}} \mathbb{E}_{\mathbb{P}} \quad (4)$$

$$\left[\min_{\mathbf{y}} \sum_{d \in \mathcal{N}_d} \left(\sum_{j \in \mathcal{N}_w} c_{dj}^w w_{dj}^c + \sum_{q \in \mathcal{N}_l} c_{dq}^l l_{dq}^s + \sum_{i \in \mathcal{N}_g} c_{di}^g p_{di}^s \right) \right] \quad (5)$$

$$s.t. \quad 0 \leq w_{dj}^c \leq \tilde{w}_{dj}, \forall d \in \mathcal{N}_d, \forall j \in \mathcal{N}_w, \quad (6)$$

$$0 \leq l_{dq}^s \leq l_{dq}, \forall d \in \mathcal{N}_d, \forall q \in \mathcal{N}_l, \quad (7)$$

$$0 \leq p_{di}^s \leq p_i, \forall d \in \mathcal{N}_d, \forall i \in \mathcal{N}_g, \quad (8)$$

$$0 \leq r_{di}^+ \leq r_{di}^{up}, \forall d \in \mathcal{N}_d, \forall i \in \mathcal{N}_g, \quad (9)$$

$$0 \leq r_{di}^- \leq r_{di}^{dn}, \forall d \in \mathcal{N}_d, \forall i \in \mathcal{N}_g, \quad (10)$$

$$-F_t \leq \sum_{i \in \mathcal{N}_g} \tau_{it}(p_i - p_{di}^s) + \sum_{j \in \mathcal{N}_w} \tau_{jt}(\tilde{w}_{dj} - w_{dj}^c) \quad (11)$$

$$- \sum_{q \in \mathcal{N}_l} \tau_{qt}(l_{dq} - l_{dq}^s) + \sum_{i \in \mathcal{N}_g} \tau_{it}(r_{di}^+ - r_{di}^-) \leq F_t, \quad (12)$$

$$\forall d \in \mathcal{N}_d, \forall t \in \mathcal{N}_t, \quad (13)$$

$$\sum_{i \in \mathcal{N}_g} (p_i - p_{di}^s) + \sum_{j \in \mathcal{N}_w} (\tilde{w}_{dj} - w_{dj}^c) + \sum_{i \in \mathcal{N}_g} (r_{di}^+ - r_{di}^-) \quad (14)$$

$$= \sum_{q \in \mathcal{N}_l} (l_{dq} - l_{dq}^s), \forall d \in \mathcal{N}_d. \quad (15)$$

Objective (4) is a two-level problem. The outer level supremum function searches for the worst wind power distribution \mathbb{P} . The inner level function minimises the RED cost under the worst-case distribution \mathbb{P} . For each sub-hourly RED process d , constraint (5) limits the amount of wind power curtailment; constraint (6) indicates the range of load shedding; constraint (7) represents the limitation of generation shedding; constraints (8) and (9) limit the utilisation of the fast-response resources within the capacity that has been purchased in DED; constraint (10) ensures the security of the transmission lines based on DC power flow model [38-41]; constraint (11) guarantees the energy balance.

2.3 Compact matrix formulation of D-SLED

To simplify the presentation, the modelling of D-SLED ((1)–(11)) is rewritten as the compact form shown by (12)–(15).

$$\min_{\mathbf{p} \in \mathcal{X}} \left\{ c(\mathbf{p}) + \sup_{\mathbb{P} \in \mathcal{P}} \mathbb{E}_{\mathbb{P}}[Q(\mathbf{p}, \tilde{\mathbf{w}})] \right\} \quad (12)$$

$$Q(\mathbf{p}, \tilde{\mathbf{w}}) = \min_{\mathbf{y}} \mathbf{d}^T \mathbf{y} \quad (13)$$

$$s.t. \quad \mathbf{T}\mathbf{p} + \mathbf{W}\mathbf{y} = \mathbf{b}, \quad (14)$$

$$\mathbf{y} \geq 0. \quad (15)$$

As the solution of $\mathbb{E}_{\mathbb{P}}[Q(\mathbf{p}, \tilde{\mathbf{w}})]$ is based on solving $Q(\mathbf{p}, \tilde{\mathbf{w}})$ considering all realisations of $\tilde{\mathbf{w}}$, the solution is computationally intractable. To handle this issue according to [31, 33, 35, 38-40], this study employs the linear decision rule in the second stage. The rule defines that \mathbf{T} , \mathbf{b} , and \mathbf{y} are affinely dependent on $\tilde{\mathbf{w}}$. As a result, the second stage based on the rule is represented by (16)–(18).

$$\mathbf{T} = \mathbf{T}(\tilde{\mathbf{w}}) = \mathbf{T}^0 + \sum_{s \in \mathcal{N}_s} \mathbf{T}^s \tilde{w}_s, \quad (16)$$

$$\mathbf{b} = \mathbf{b}(\tilde{\mathbf{w}}) = \mathbf{b}^0 + \sum_{s \in \mathcal{N}_s} \mathbf{b}^s \tilde{w}_s, \quad (17)$$

$$\mathbf{y} = \mathbf{y}(\tilde{\mathbf{w}}) = \mathbf{y}^0 + \sum_{s \in \mathcal{N}_s} \mathbf{y}^s \tilde{w}_s, \quad (18)$$

$$\begin{aligned} \tilde{\mathbf{w}} &= [\tilde{w}_{11}, \dots, \tilde{w}_{1|\mathcal{N}_w|}, \\ &\quad \tilde{w}_{21}, \dots, \tilde{w}_{2|\mathcal{N}_w|}, \dots, \\ &\quad \tilde{w}_{|\mathcal{N}_d|1}, \dots, \tilde{w}_{|\mathcal{N}_d||\mathcal{N}_w|}]^T \\ &= [\tilde{w}_1, \dots, \tilde{w}_{|\mathcal{N}_s|}]^T, |\mathcal{N}_s| = |\mathcal{N}_w| \times |\mathcal{N}_d|. \end{aligned} \quad (19)$$

The presented linear decision rule is, to some extent, a linear approximation of the nonlinear relationship between $(\mathbf{T}, \mathbf{b}, \mathbf{y})$ and $\tilde{\mathbf{w}}$, whose accuracy has been proven to be acceptable [38-40]. Although it inevitably introduces a certain conservatism to the model, it can bring significant computational tractability and scalability.

3 Reformulation of D-SLED with WKS-format ambiguity set

3.1 Statistic information obtained from historical data

This subsection presents the extraction of statistic information from historical data. The ambiguity set construction in DRO is based on the extracted statistic information.

$$w_s^{min} \leq \tilde{w}_s \leq w_s^{max}, \forall s \in \mathcal{N}_s, \quad (20)$$

$$\mathbb{E}_{\mathbb{P}'}[\tilde{w}_s] = \mu_s, \forall s \in \mathcal{N}_s, \quad (21)$$

$$\mathbb{E}_{\mathbb{P}'}[\tilde{w}_s^2] \leq \sigma_s, \forall s \in \mathcal{N}_s, \quad (22)$$

$$\mathbb{E}_{\mathbb{P}'}[\tilde{w}_s^3] \leq \xi_s, \forall s \in \mathcal{N}_s. \quad (23)$$

For the uncertain wind power generation \tilde{w}_s under a certain distribution \mathbb{P}' , inequality (20) provides a prediction interval, equation (21) indicates that the mean of the predicted generation is μ_s , inequality (22) reveals that the quadratic value of the predicted generation is no higher than σ_s , and inequality (23) indicates that the cubic value of the predicted generation is less than or equal to ξ_s .

3.2 General ambiguity set construction

Based on the statistic information given by (20)–(23), for an uncertain wind power vector $\tilde{\mathbf{w}} \in \mathbb{R}^{|\mathcal{N}_s|}$, a general ambiguity set \mathcal{P}' containing a family of wind power distributions can be constructed using (24).

$$\mathcal{P}' = \left\{ \mathbb{P}' \in \mathcal{P}_0(\tilde{\mathbf{w}} \in \mathbb{R}^{|\mathcal{N}_s|}) : \begin{array}{l} \Omega' : \{\tilde{\mathbf{w}} \in [\mathbf{w}^{min}, \mathbf{w}^{max}]\} \\ \mathbb{P}'[\tilde{\mathbf{w}} \in \Omega'] = 1 \\ \mathbb{E}_{\mathbb{P}'}[\tilde{\mathbf{w}}] = \boldsymbol{\mu} \\ \mathbb{E}_{\mathbb{P}'}[\tilde{\mathbf{w}}^2] \leq \boldsymbol{\sigma} \\ \mathbb{E}_{\mathbb{P}'}[\tilde{\mathbf{w}}^3] \leq \boldsymbol{\xi} \end{array} \right\} \quad (24)$$

The interval and first-order expectation information in \mathcal{P}' provide the basis for wind power prediction. Additionally, higher-order information represents the quality of the basis according to the degree of information dispersion.

3.3 Lifting the general ambiguity set to WKS-format ambiguity

The high-order information terms, including the quadratic and cubic terms of (24), prevent the effective solution of D-SLED. Therefore, the *lifting theorem* [32, 33] is adopted to lift the general ambiguity set to a WKS-format ambiguity (25) set such that *Lemma 1* can be employed to solve D-SLED. The details of the *lifting theorem* are provided in Appendix 7.1 while the construction process is provided in Appendix 7.2.

$$\begin{aligned} \mathcal{P} &= \left\{ \mathbb{P} \in \mathcal{P}_0(\begin{array}{c} \tilde{\mathbf{w}} \in \mathbb{R}^{|\mathcal{N}_s|} \\ \tilde{\mathbf{u}} \in \mathbb{R}^{|\mathcal{N}_s|} \end{array}) : \begin{array}{l} \Omega = \{C_s \tilde{\mathbf{w}} + D_s \tilde{\mathbf{u}} \succeq_{\mathcal{K}_s} f_s\} \\ \mathbb{P}[(\tilde{\mathbf{w}}, \tilde{\mathbf{u}}) \in \Omega] = 1 \\ \mathbb{E}_{\mathbb{P}}[A \tilde{\mathbf{w}} + B \tilde{\mathbf{u}}] = e \end{array} \right\} \\ \mathbf{A} &= \begin{bmatrix} \mathbf{E}_{|\mathcal{N}_s|} \\ 0 \end{bmatrix}_{2|\mathcal{N}_s| \times |\mathcal{N}_s|}, \mathbf{B} = \begin{bmatrix} 0 \\ \mathbf{E}_{|\mathcal{N}_s|} \end{bmatrix}_{2|\mathcal{N}_s| \times |\mathcal{N}_s|}, \\ \mathbf{C}_0 &= \begin{bmatrix} \mathbf{E}_{|\mathcal{N}_s|} \\ -\mathbf{E}_{|\mathcal{N}_s|} \end{bmatrix}_{2|\mathcal{N}_s| \times |\mathcal{N}_s|}, \\ \mathbf{D}_0 &= 0, \\ \mathbf{e} &= \begin{bmatrix} \boldsymbol{\mu} \\ \boldsymbol{\sigma} \end{bmatrix}_{2|\mathcal{N}_s| \times 1}, \\ \mathbf{C}_s &= \begin{bmatrix} & & & \overset{s^{th}}{\underbrace{1}} & 0 & \cdots & 0 \\ 0 & \cdots & 0 & 0 & 0 & \cdots & 0 \\ 0 & \cdots & 0 & 0 & 0 & \cdots & 0 \\ 0 & \cdots & 0 & 0 & 0 & \cdots & 0 \end{bmatrix}_{3 \times |\mathcal{N}_s|}, \\ \mathbf{D}_s &= \begin{bmatrix} & & & \overset{s^{th}}{\underbrace{0}} & 0 & \cdots & 0 \\ 0 & \cdots & 0 & 0 & 0 & \cdots & 0 \\ 0 & \cdots & 0 & 1/2 & 0 & \cdots & 0 \\ 0 & \cdots & 0 & 1/2 & 0 & \cdots & 0 \end{bmatrix}_{3 \times |\mathcal{N}_s|}, \\ \mathbf{f}_0 &= \begin{bmatrix} \mathbf{w}^{min} \\ -\mathbf{w}^{max} \end{bmatrix}_{2|\mathcal{N}_s| \times 1}, \mathbf{f}_s = \begin{bmatrix} 0 \\ 1/2 \\ -(1/2) \end{bmatrix}_{3 \times 1}, \\ \mathcal{K}_0 &= \mathbb{R}_+^{2|\mathcal{N}_s| \times 1}, \mathcal{K}_s = \mathbb{L}^3, s = 0, 1, 2, \dots, |\mathcal{N}_s|. \end{aligned} \quad (25)$$

Equation (25) represents a second-order WKS-format ambiguity set containing interval, first-order, and second-order information. Unlike the initial ambiguity set \mathcal{P}' , \mathcal{P} can preserve available wind power statistical information, such as prediction intervals, first-order information, and even higher-order information, in the unified conic format rather than in different formats. Therefore, \mathcal{P} possesses flexible high-order information utilisation capacity (order-utilisation ability), which potentially balances optimism and conservatism. Additionally, \mathcal{P} is proved to be more tractable than \mathcal{P}' .

It should be pointed out that although third-order is the highest order of information employed in this paper, only the reformulation process of the second-order ambiguity set is provided, because the second-order set is the most general in terms of practical application. Additionally, the reformulations for ambiguity sets with different orders follow the same general methodology and their details have been provided in [33].

3.4 Reformulation of D-SLED using Lemma 1

To solve min-sup-min D-SLED effectively, *Theorem 1* of [33] is employed, which is summarised as *Lemma 1*.

Lemma 1: Under the linear decision rule ((16)–(18)) with WKS-format ambiguity set (25), the second-stage RED ((13)–(15)) as a linear program (LP) can be equivalently reformulated to the conic optimisation problem given by (26).

$$\begin{aligned}
& \sup_{\mathbb{P} \in \mathcal{P}} \mathbb{E}_{\mathbb{P}} \left[\min_{\mathbf{y}} \mathbf{d}^T (\mathbf{y}^0 + \sum_{s \in \mathcal{N}_s} \mathbf{y}^s \tilde{w}_s) \right] \\
& \text{s.t. } \mathbf{T}(\tilde{\mathbf{w}})\mathbf{p} + \mathbf{W}\mathbf{y}(\tilde{\mathbf{w}}) = \mathbf{b}(\tilde{\mathbf{w}}), \\
& \quad \mathbf{T}(\tilde{\mathbf{w}}) = \mathbf{T}^0 + \sum_{s \in \mathcal{N}_s} \mathbf{T}^s \tilde{w}_s, \\
& \quad \mathbf{y}(\tilde{\mathbf{w}}) = \mathbf{y}^0 + \sum_{s \in \mathcal{N}_s} \mathbf{y}^s \tilde{w}_s, \\
& \quad \mathbf{b}(\tilde{\mathbf{w}}) = \mathbf{b}^0 + \sum_{s \in \mathcal{N}_s} \mathbf{b}^s \tilde{w}_s, \\
& \quad \mathbf{y}(\tilde{\mathbf{w}}) \geq 0. \\
& \Leftrightarrow \min_{\mathbf{Y}, \mathcal{L}, \boldsymbol{\alpha}, \beta, \boldsymbol{\varphi}} [\mathbf{e}^T \boldsymbol{\alpha} + \beta] \\
& \text{s.t. } \mathbf{T}^s \mathbf{p} + \mathbf{W}\mathbf{y}^s = \mathbf{b}^s, \\
& \quad \mathbf{C}^T \boldsymbol{\varphi} = \mathbf{A}^T \boldsymbol{\alpha} - \mathbf{Y}^{0^T} \mathbf{d}, \\
& \quad \mathbf{D}^T \boldsymbol{\varphi} = \mathbf{B}^T \boldsymbol{\alpha}, \\
& \quad \mathbf{C}^T \mathbf{L}^v = \mathbf{y}_v, \\
& \quad \mathbf{D}^T \mathbf{L}^v = 0, \\
& \quad \mathbf{f}^T \boldsymbol{\varphi} - \mathbf{d}^T \mathbf{y}^0 + \beta \geq 0, \\
& \quad \mathbf{y}_v^0 + \mathbf{f}^T \mathbf{L}^v \geq 0, \\
& \quad \mathbf{Y} = [\mathbf{y}^0, \mathbf{y}^1, \dots, \mathbf{y}^{|\mathcal{N}_s|}], \\
& \quad = [\mathbf{y}^0, \mathbf{Y}^0] \in \mathbb{R}^{|\mathcal{N}_y|} \times \mathbb{R}^{|\mathcal{N}_y| \times |\mathcal{N}_s|}, \\
& \quad \mathbf{y}_v = [y_v^1, \dots, y_v^{|\mathcal{N}_s|}]^T \in \mathbb{R}^{|\mathcal{N}_s| \times 1}, \\
& \quad \mathcal{L} = [\mathbf{L}^1, \dots, \mathbf{L}^{|\mathcal{N}_y|}] \in \mathbb{R}^{3 \times |\mathcal{N}_y|}, \\
& \quad \boldsymbol{\alpha} \in \mathbb{R}^{2|\mathcal{N}_s| \times 1}, \beta \in \mathbb{R}, \boldsymbol{\varphi} \in \mathbb{L}^3, \mathbf{L}^v \in \mathbb{L}^3, \\
& \quad \forall v \in \mathcal{N}_y, \forall s \in \mathcal{N}_s, \forall i \in \mathcal{N}_g. \tag{26}
\end{aligned}$$

Conic optimisation problem (26) leads to the final formulated D-SLED (27).

Table 1 Characteristics of the four cases.

Cases	Characteristics of Wind Power	Condition
1	Sufficient	Winter, from 7 p.m. to 8 p.m.
2	Insufficient	Summer, from 1 p.m. to 2 p.m.
3	Decreases over time	Wind fluctuates from fast to slow
4	Increases over time	Wind fluctuates from slow to fast

$$\begin{aligned}
& \min_{\mathbf{p}, \mathbf{Y}, \mathcal{L}, \boldsymbol{\alpha}, \beta, \boldsymbol{\varphi}} \left\{ \sum_{i \in \mathcal{N}_g} \left[a_i(p_i)^2 + b_i p_i \right] + \mathbf{e}^T \boldsymbol{\alpha} + \beta \right\} \\
& \text{s.t. } p_i^{min} \leq p_i \leq p_i^{max}, \\
& R_i^{dn} \leq p_i - p_i^0 \leq R_i^{up}, \\
& \mathbf{T}^s \mathbf{p} + \mathbf{W}\mathbf{y}^s = \mathbf{b}^s, \\
& \mathbf{C}^T \boldsymbol{\varphi} = \mathbf{A}^T \boldsymbol{\alpha} - \mathbf{Y}^{0^T} \mathbf{d}, \\
& \mathbf{D}^T \boldsymbol{\varphi} = \mathbf{B}^T \boldsymbol{\alpha}, \\
& \mathbf{C}^T \mathbf{L}^v = \mathbf{y}_v, \\
& \mathbf{D}^T \mathbf{L}^v = 0, \\
& \mathbf{f}^T \boldsymbol{\varphi} - \mathbf{d}^T \mathbf{y}^0 + \beta \geq 0, \\
& \mathbf{y}_v^0 + \mathbf{f}^T \mathbf{L}^v \geq 0, \\
& \mathbf{Y} = [\mathbf{y}^0, \mathbf{y}^1, \dots, \mathbf{y}^{|\mathcal{N}_s|}], \\
& = [\mathbf{y}^0, \mathbf{Y}^0] \in \mathbb{R}^{|\mathcal{N}_y|} \times \mathbb{R}^{|\mathcal{N}_y| \times |\mathcal{N}_s|}, \\
& \mathbf{y}_v = [y_v^1, \dots, y_v^{|\mathcal{N}_s|}]^T \in \mathbb{R}^{|\mathcal{N}_s| \times 1}, \\
& \mathcal{L} = [\mathbf{L}^1, \dots, \mathbf{L}^{|\mathcal{N}_y|}] \in \mathbb{R}^{3 \times |\mathcal{N}_y|}, \\
& \boldsymbol{\alpha} \in \mathbb{R}^{2|\mathcal{N}_s| \times 1}, \beta \in \mathbb{R}, \boldsymbol{\varphi} \in \mathbb{L}^3, \mathbf{L}^v \in \mathbb{L}^3, \\
& \forall v \in \mathcal{N}_y, \forall s \in \mathcal{N}_s, \forall i \in \mathcal{N}_g. \tag{27}
\end{aligned}$$

Finally, based on the linear decision rule and WKS-format ambiguity set, *Lemma 1* enables D-SLED models with different orders to be reformulated as the unified conic models (27) that can be directly solved by commercial solvers.

4 Experimental result

4.1 Experimental setting

The IEEE 118-bus system with 186 lines, 54 generators, and 8 wind power generators (WPGs) is employed for the experiments. The parameter settings are provided in Appendix 7.3 Table 5. Four typical hourly cases from Southwest China are selected to evaluate and validate the effectiveness of D-SLED. The details of the cases are summarized in Table 1 and Appendix 7.4 Fig. 8.

The dispatch horizon is 1 h [14]. Dispatch decisions include LED strategy \mathbf{p} and RED strategy $\mathbf{y} = \{w^c, l^s, p^s, r^+, r^-\}$. The LED strategy will be implemented by the generators while the RED results merely serve for performance evaluation. The details of the experimental environment and performance evaluation are listed in Table 2.

4.2 Investigating the economy of SLED

The performances of 10-min, 20-min, 30-min, and 60-min resolution models are evaluated and compared. Based on a Gaussian distribution with 15% root mean square error [14], a Monte Carlo simulation (MCS) generates 1000 scenarios to construct the WKS-format ambiguity set with the interval and the first-order information. Another 3000 scenarios are generated for evaluation. Fig. 3 illustrates the

Table 2 Details of the experimental environment and optimisation evaluation.

Experimental Environment

CPU: Corei3-7100@3.0 GHz.

RAM: 4 GB.

Platform: MATLAB 2016.

Solvers: CPLEX for LP and mixed integer LP, MOSEK for convex optimisation.

Optimisation Phase

Step 1: Set maximum prediction error for Monte Carlo simulation (MCS).

Step 2: MCS generates a number of historical scenarios using the four cases, in which the order information is obtained.

Step 3: Solve the problems (27). Record the expected total operational cost, the first-stage decision p , the first-stage cost $c(p)$, and solving time. The expected total cost of the problem (27) provides the optimism degree of the optimisation.

Evaluation Phase

Step 4: Based on the same prediction error assumptions, MCS generates the testing scenarios.

Step 5: Input p into the second-stage problem (13)–(15). Solve the second-stage problem for each testing scenario. Record each actual second-stage decision and the average second-stage cost of all test scenarios.

Step 6: Add the average second-stage cost to the first-stage cost $c(p)$, to obtain the actual total operational cost. The economy of the optimisation can be evaluated based on the actual total cost.

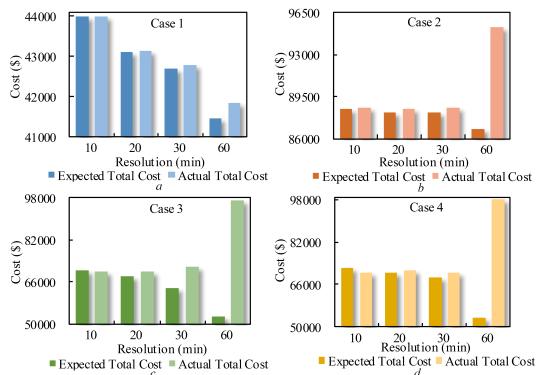


Fig. 3: Comparison of the influence of different resolutions on costs.

relationship between cost and resolution. In the four cases, the expected total cost of SLED is higher than that of HLED. As higher expected total cost signifies more conservativeness optimisation results, Fig. 3 indicates that the finer models are more conservative than the rougher models. The difference in conservativeness occurs because the finer models consider the sub-hourly wind power fluctuations in the dispatch horizon more comprehensively, while rougher models roughly average the fluctuations. As a result, finer models provide a more conservative LED strategy to handle the sub-hourly fluctuations at different time points. Contrarily, rougher models, especially 60-min models, lead to a more optimistic strategy because the models optimistically consider that the wind power in the dispatch horizon is relatively average and stable. Although the conservative strategy increases the actual total cost in case 1, it reduces the actual cost in cases 2, 3, and 4. The differences in the actual cost trends owe to the different characteristics of the cases. Specifically, the wind power in case 1 is sufficient and stable while that of cases 2, 3, and 4 is insufficient or fluctuating. As a result, the conservative strategy of the rougher models results in lower economy in case 1 but significantly improves the economy in cases 2, 3, and 4.

Fig. 4 further shows that the load shedding probability of SLED is always lower than that of HLED in the four cases. Because the probability is an important index of robustness, this result strongly indicates that SLED can provide better robustness.

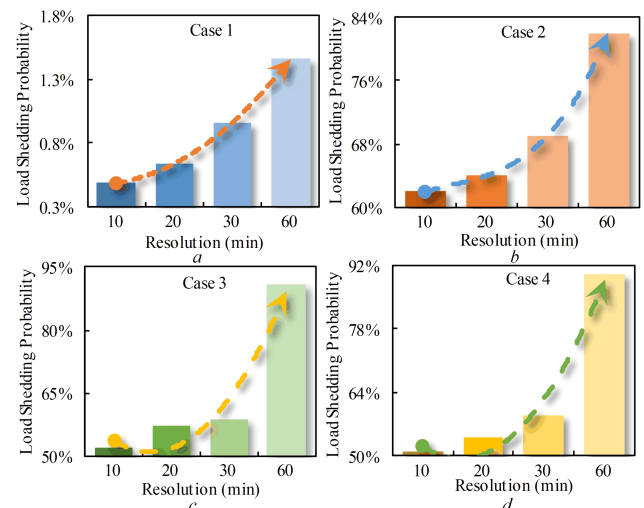


Fig. 4: Comparison of the effect of different resolutions on load shedding.

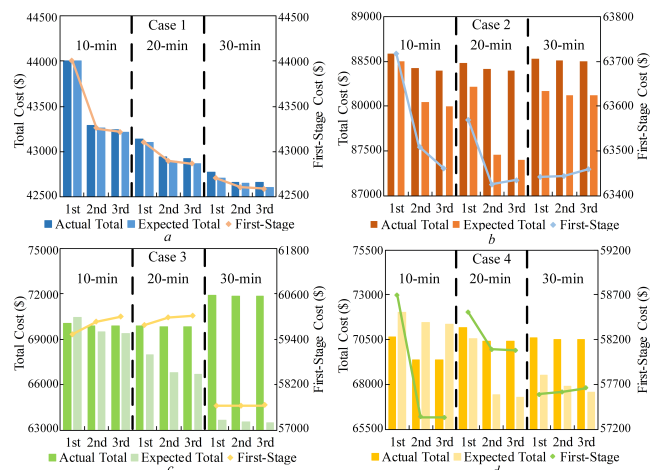


Fig. 5: Comparison of the costs of D-SLED with different order-utilisation levels.

These models are represented as equation (27), where 1st-order indicates that the ambiguity set comprises interval and first-order information; 2nd-order indicates that the ambiguity set comprises interval, first-order, and second-order information; and 3rd-order indicates that the ambiguity set comprises interval, first-order, second-order, and third-order information.

4.3 Evaluating the economic benefits from the order-utilisation ability of D-SLED

To evaluate the economic benefits from the order-utilisation ability, D-SLED models based on first-order, second-order, and third-order ambiguity sets are compared using models with the same resolution; the results are shown in Fig. 5. The line charts illustrate that in models with the same resolution, higher-order information results in first-stage strategies with different levels of conservativeness. Specifically, although some outliers exist, the conservativeness of the first-stage strategy with higher-order information generally tends to be lower in cases 1, 2, and 4; the conservativeness of the first-stage strategy with higher-order information increases in case 3. In terms of the expected cost, the histograms demonstrate that for the models with the same resolution, the expected cost with higher-order information becomes lower in all four cases. Moreover, the histograms also indicate that in all four cases, utilising higher-order information reduces the actual total costs in terms of the models with the same resolution. The lowest actual and expected costs are achieved in cases where the third-order information is utilised.

Table 3 Comparison of D-SLED and S-SLED.

Resolution	Method	Scenarios	Time (s)	Total Cost (\$)		Actual Total Cost Interval
				Expected	Actual	
10 min	S-SLED	50	399.16	39234.48	42827.72	[42784.66, 46127.25]
		500	1269.90	41262.99	42361.16	[42242.66, 47169.27]
	D-SLED	50	402.12	44137.44	44147.78	[44035.21, 44197.49]
		500	392.92	43924.71	43930.51	[43876.65, 44047.43]
20 min	S-SLED	50	66.67	38645.89	42827.72	[42284.06, 46627.35]
		500	301.46	40544.44	42606.03	[42424.65, 47819.36]
	D-SLED	50	76.86	43998.44	43999.32	[43989.11, 45021.53]
		500	71.86	43149.56	43279.06	[43259.21, 45214.91]
30 min	S-SLED	50	39.45	33969.90	43096.58	[38842.86, 63759.25]
		500	285.26	34950.40	42629.43	[40964.54, 53845.66]
	D-SLED	50	53.42	43098.33	43225.60	[43098.22, 47524.44]
		500	51.14	43024.15	42934.97	[42898.22, 47908.94]

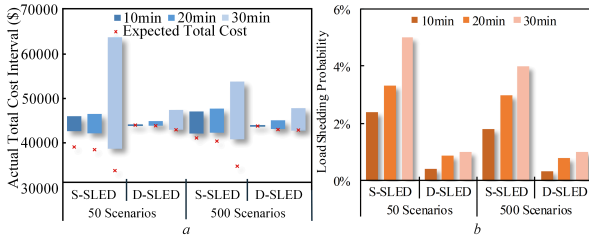


Fig. 6: Comparison of S-SLED and D-SLED.

a Difference between the total cost interval of S-SLED and D-SLED.
b Load shedding probability of S-SLED and D-SLED.

These outcomes occur because the ambiguity sets with higher-order information can comprehensively capture the wind power distribution to achieve more appropriate first-stage strategies for different cases. Further, more comprehensive wind power distribution allows the optimisation to be optimistic, so that the expected cost is lower. In terms of the economic benefits, the actual cost results indicate that the strategy with higher-order information achieves economic improvement. As a result, it can be concluded that the order-utilisation ability can help D-SLED to improve the economy of operation.

Additionally, as finer models consider the sub-hourly fluctuations accurately, the improvement in the economy resulting from the order-utilisation ability is more significant in finer models, especially in 10-min resolution SLED. This proves that it is significantly appropriate to apply the order-utilisation ability of WKS-type DRO to SLED.

4.4 Comparison of solution methods

4.4.1 Comparison of D-SLED and S-SLED: Based on the Gaussian distribution with 15% root mean square error [14], 50 and 500 scenarios are generated based on case 1 for optimisation while 1500 scenarios are generated for evaluation. The experimental results are listed in Table 3. Under the assumption that the distribution can appropriately capture the uncertainty, the table indicates that to immunise the thermal generation plan against the worst-case distribution, the actual total cost of D-SLED is generally higher than that of S-SLED with the same resolution and number of scenarios. However, S-SLED strongly relies on the large-size scenarios to reduce the actual total cost. Therefore, computational efficiency decreases as the number of scenarios increases. In contrast, the computational efficiency of D-SLED in Table 3 is influenced by the resolution but not by the number of scenarios. Hence, computational efficiency can be ensured.

Fig. 6(a) shows that although the actual total cost interval of D-SLED is short, D-SLED ensures that the expected total cost lies within the interval. This result proves that D-SLED can provide appropriate expected total cost. In contrast, S-SLED cannot ensure

Table 4 Comparison of computational efficiencies of D-SLED and A-SLED.

Maximum Prediction Error	D-SLED (s)	A-SLED (s)		
		$\Gamma = 6$	$\Gamma = 10$	$\Gamma = 14$
15%	55.29	19.79	36.56	49.54
20%	54.22	17.00	26.67	59.45
25%	61.30	21.32	29.45	63.49

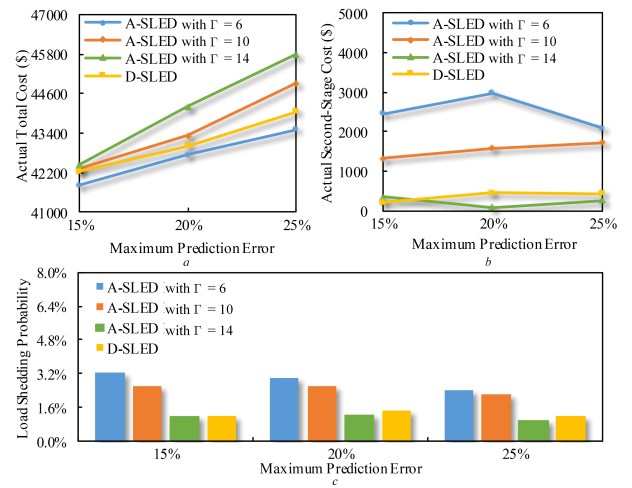


Fig. 7: Comparison of A-SLED and D-SLED.

a Comparison of the actual total cost.

b Comparison of the actual second-stage cost.

c Comparison of the load shedding probability.

the expected total cost within the interval, which indicates that S-SLED is over-optimistic. Fig. 6(b) further shows that S-SLED relies on the large-size scenario to decrease the load shedding probability. However, the probability of D-SLED remains almost the same even when the number of scenarios decreases from 500 to 50. Moreover, the probability of D-SLED is generally lower than that of S-SLED. The load shedding improvement owes to the fact that D-SLED employs order information rather than large-size scenarios to capture the worst-case distribution. As a result, the robustness of D-SLED outperforms S-SLED in terms of stability and overall performance.

4.4.2 Comparison of D-SLED and A-SLED: The formulation and solution method of A-SLED are briefly provided in Appendix 7.5. According to the formulation, the uncertainty set of A-SLED has the same interval structure as the initial support set Ω' of D-SLED. Both sets are constructed using maximum prediction errors of 15%, 20%, and 25%. The following experiments are based on 30-min models. In A-SLED, the budget parameter Γ determines the conservative level of the optimisation, and it varies from 0 to

16. In our experiments, budgets $\Gamma = 6, 10$, and 14 are employed for comparison, which represent three worst-case scenarios with different pessimistic degrees.

According to Table 4, although the computational efficiency of A-SLED with $\Gamma = 6$ and 10 is higher than that of D-SLED, both models are comparable in terms of solving time. Fig. 7(a) shows that the actual total costs of A-SLED with $\Gamma = 10$ and 14 are higher than those of D-SLED. This is because D-SLED only focuses on the worst distribution instead of the worst scenario. As a result, a more economical solution can be achieved using D-SLED.

Fig. 7(b) and Fig. 7(c) further compare the robustness. Fig. 7(b) demonstrates that the actual second-stage RED costs of A-SLED with $\Gamma = 6$ and 10 are higher than those of D-SLED. As the robustness partly reflects on cost of RED, Fig. 7(b) indicates that D-SLED is more robust than A-SLED with $\Gamma = 6$ and 10 while less robust than A-SLED with $\Gamma = 14$. In this regard, as Fig. 7(c) illustrates, the reason is that the load shedding probability of D-SLED is between that of A-SLED with $\Gamma = 10$ and that of A-SLED with $\Gamma = 14$.

5 Conclusion

This paper presents a DRO-based two-stage sub-hourly LED model to obtain the optimal LED strategy considering wind power uncertainty. The model considers sub-hourly fluctuations in wind power to develop an accurate dispatch strategy. Before the realisation of wind power uncertainty, the hourly first stage provides a look-ahead thermal generator output plan according to the worst wind power distribution. Then, the sub-hourly second stage implements the fast-response operation to correct the look-ahead strategy as long as the uncertainty of wind power is realised. A novel WKS-format ambiguity set is constructed using the *lifting theorem*. The ambiguity set can fully utilise historical statistic information, including interval, mean, quadratic, cubic, and higher-order information, to obtain a family of wind power distributions. Therefore, the look-ahead strategy can withstand the worst-case distribution in the ambiguity set. Based on the unified conic formulation of the WKS-format ambiguity set and the linear decision rule, D-SLED can be converted into a tractable conic optimisation problem using *Lemma 1* such that D-SLED can be effectively and directly solved. The experimental results indicate the effectiveness of the presented D-SLED. Compared with the conventional HLED model, the presented model achieves significant economy and robustness improvements. Case studies indicate that WKS-type DRO outperforms SO and ARO in terms of balancing economy, robustness, and computational efficiency. Our future work will further consider security constraints and the multiple uncertainties of solar power and load demand, and then execute LED optimisation in a dynamic receding horizon.

6 References

- [1] Khodayar, M., Wu, L., Shahidehpour, M.: 'Hourly coordination of electric vehicle operation and volatile wind power generation in SCUC', *IEEE Trans. Smart Grid*, 2012, **3**, (3), pp. 1271–1279
- [2] Jabr, R., Pal, B.: 'Intermittent wind generation in optimal power flow dispatching', *IET Gener. Transm. Distrib.*, 2009, **3**, (1), pp. 66–74
- [3] Kamalinia, S., Shahidehpour, M.: 'Generation expansion planning in wind-thermal power systems', *IET Gener. Transm. Distrib.*, 2010, **4**, (8), pp. 940–951
- [4] Qin, M., Chan, K., Chung, C., Luo, X., Wu, T.: 'Optimal planning and operation of energy storage systems in radial networks for wind power integration with reserve support', *IET Gener. Transm. Distrib.*, 2016, **10**, (8), pp. 2019–2025
- [5] Wu, L., Shahidehpour, M., Li, T.: 'Stochastic security-constrained unit commitment', *IEEE Trans. Power Syst.*, 2007, **22**, (2), pp. 800–811
- [6] Wu, L., Shahidehpour, M., Li, T.: 'Cost of reliability analysis based on stochastic unit commitment', *IEEE Trans. Power Syst.*, 2008, **23**, (3), pp. 1364–1374
- [7] Wu, L., Shahidehpour, M., Fu, Y.: 'Security-constrained generation and transmission outage scheduling with uncertainties', *IEEE Trans. Power Syst.*, 2010, **25**, (3), pp. 1674–1685
- [8] Li, Z., Wu, W., Zhang, B., Wang, B.: 'Adjustable robust real-time power dispatch with large-scale wind power integration', *IEEE Trans. Sustain. Energy*, 2015, **6**, (2), pp. 357–368
- [9] Hetzer, J., Yu, D., Bhattacharai, K.: 'An economic dispatch model incorporating wind power', *IEEE Trans. Energy Convers.*, 2008, **23**, (2), pp. 603–611
- [10] Zhang, Z., Sun, Y., Gao, D., Lin, J., Cheng, L.: 'A versatile probability distribution model for wind power forecast errors and its application in economic dispatch', *IEEE Trans. Power Syst.*, 2013, **28**, (3), pp. 3114–3125
- [11] Yang, Y., Zhai, Q., Guan, X.: 'An hour-ahead scheduling problem for a system with wind resource', *Proc. IEEE PES General Meeting*, San Diego, United States, July 2012, pp. 1–8
- [12] Wu, W., Chen, J., Zhang, B., Sun, H.: 'A robust wind power optimization method for look-ahead power dispatch', *IEEE Trans. Sustain. Energy*, 2014, **5**, (2), pp. 507–515
- [13] Xie, L., Gu, Y., Zhu, X., Genton, M.: 'Short-term spatio-temporal wind power forecast in robust look-ahead power system dispatch', *IEEE Trans. Smart Grid*, 2013, **5**, (1), pp. 511–520
- [14] Wei, W., Liu, F., Mei, S.: 'Distributionally robust co-optimization of energy and reserve dispatch', *IEEE Trans. Sustain. Energy*, 2016, **7**, (1), pp. 289–300
- [15] Chen, Y., Wei, W., Liu, F., Mei, S.: 'Distributionally robust hydro-thermal-wind economic dispatch', *Appl. Energy*, 2016, **173**, pp. 511–519
- [16] Gangammanavar, H., Sen, S., Zavala, V.: 'Stochastic optimization of sub-hourly economic dispatch with wind energy', *IEEE Trans. Power Syst.*, 2016, **31**, (2), pp. 949–959
- [17] Gangammanavar, H., Sen, S.: 'Two-scale stochastic optimization for controlling distributed storage devices', *IEEE Trans. Smart Grid*, 2018, **9**, (4), pp. 2691–2702
- [18] Ela, E., O'Malley, M.: 'Studying the variability and uncertainty impacts of variable generation at multiple timescales', *IEEE Trans. Power Syst.*, 2012, **27**, (3), pp. 1324–1333
- [19] Zhihuan, L., Yinhong, L., Xianzhong, D.: 'Non-dominated sorting genetic algorithm-II for robust multi-objective optimal reactive power dispatch', *IET Gener. Transm. Distrib.*, 2010, **4**, (9), pp. 1000–1008
- [20] Wong, K., Fung, C.: 'Simulated annealing based economic dispatch algorithm', *IEE P. C (IET Gener. Transm. Distrib.)*, 1993, **140**, (6), pp. 509–515
- [21] El-Zonkoly, A.: 'Optimal placement of multi-distributed generation units including different load models using particle swarm optimisation', *IET Gener. Transm. Distrib.*, 2011, **5**, (7), pp. 760–771
- [22] Niknam, T., Narimani, M., Aghaei, J., Azizipanah-Abarghooee, R.: 'Improved particle swarm optimisation for multi-objective optimal power flow considering the cost, loss, emission and voltage stability index', *IET Gener. Transm. Distrib.*, 2012, **6**, (6), pp. 515–527
- [23] Liu, C., Shahidehpour, M., Fu, Y., Li, Z.: 'Security-constrained unit commitment with natural gas transmission constraints', *IEEE Trans. Power Syst.*, 2009, **24**, (3), pp. 1523–1536
- [24] Correa-Posada, C., Sánchez-Martín, P.: 'Integrated power and natural gas model for energy adequacy in short-term operation', *IEEE Trans. Power Syst.*, 2014, **30**, (6), pp. 3347–3355
- [25] Liu, Y., Nair, N.: 'A two-stage stochastic dynamic economic dispatch model considering wind uncertainty', *IEEE Trans. Sustain. Energy*, 2015, **7**, (2), pp. 819–829
- [26] Soares, J., Canizes, B., Ghazvini, M., Vale, Z., Venayagamoorthy, G.: 'Two-stage stochastic model using benders decomposition for large-scale energy resource management in smart grids', *IEEE Trans. Ind. Appl.*, 2017, **53**, (6), pp. 5905–5914
- [27] He, C., Wu, L., Liu, T., Shahidehpour, M.: 'Robust co-optimization scheduling of electricity and natural gas systems via ADMM', *IEEE Trans. Sustain. Energy*, 2016, **8**, (2), pp. 658–670
- [28] Zhao, C., Jiang, R.: 'Distributionally robust contingency-constrained unit commitment', *IEEE Trans. Power Syst.*, 2017, **33**, (1), pp. 94–102

- [29] Delage, E., Ye, Y.: 'Distributionally robust optimization under moment uncertainty with application to data-driven problems', *Oper. Res.*, 2010, **58**, (3), pp. 595–612
- [30] Wei, W., Wang, J., Mei, S.: 'Dispatchability maximization for co-optimized energy and reserve dispatch with explicit reliability guarantee', *IEEE Trans. Power Syst.*, 2015, **31**, (4), pp. 3276–3288
- [31] Alismail, F., Xiong, P., Singh, C.: 'Optimal wind farm allocation in multi-area power systems using distributionally robust optimization approach', *IEEE Trans. Power Syst.*, 2017, **33**, (1), pp. 536–544
- [32] Wiesemann, W., Kuhn, D., Sim, M.: 'Distributionally robust convex optimization', *Oper. Res.*, 2014, **62**, (6), pp. 1358–1376
- [33] Li, B., Qian, X., Sun, J., Teo, K., Yu, C.: 'A model of distributionally robust two-stage stochastic convex programming with linear recourse', *Appl. Math. Model.*, 2018, **58**, pp. 86–97
- [34] Ben-Tal, A., Goryashko, A., Guslitzer, E., Nemirovski , A.: 'Adjustable robust solutions of uncertain linear programs', *Math. Program.*, 2004, **99**, (2), pp. 351–376
- [35] Lu, X., Chan, K. W., Xia, S., Zhou, B., Luo, X.: 'Security-constrained multiperiod economic dispatch with renewable energy utilizing distributionally robust optimization', *IEEE Trans. Sustain. Energy*, 2018, **10**, (2), pp. 768–779
- [36] Shen, X., Liu, Y., Liu, Y.: 'A multistage solution approach for dynamic reactive power optimization based on interval uncertainty', *Math. Probl. Eng.*, 2018, **2018**, DOI: 10.1155/2018/3854812
- [37] Wei, P., Liu, Y.: 'The integration of wind-solar-hydropower generation in enabling economic robust dispatch', *Math. Probl. Eng.*, 2019, **2019**, DOI: 10.1155/2019/4634131
- [38] Duan, C., Jiang, L., Fang, W., Liu, J.: 'Data-driven affinely adjustable distributionally robust unit commitment', *IEEE Trans. Power Syst.*, 2017, **33**, (2), pp. 1385–1398
- [39] Duan, C., Jiang, L., Fang, W., Liu, J., Liu, S.: 'Data-driven distributionally robust energy-reserve-storage dispatch', *IEEE Trans. Ind. Inform.*, 2017, **14**, (7), pp. 2826–2836
- [40] Xiong, P., Jirutitijaroen, P., Singh, C.: 'A distributionally robust optimization model for unit commitment considering uncertain wind power generation', *IEEE Trans. Power Syst.*, 2016, **32**, (1), pp. 39–49
- [41] Yao, L., Wang, X., Duan, C., Guo, J., Wu, X., Zhang, Y.: 'Data-driven distributionally robust reserve and energy scheduling over Wasserstein balls', *IET Gener. Transm. Distrib.*, 2017, **12**, (1), pp. 178–189
- [42] Gao, H., Wang, L., Liu, J., Wei, Z.: 'Integrated day-ahead scheduling considering active management in future smart distribution system', *IEEE Trans. Power Syst.*, 2018, **33**, (6), pp. 6049–6061
- [43] Chen, Y., Guo, Q., Sun, H., Li, Z., Wu, W., Li, Z.: 'A distributionally robust optimization model for unit commitment based on Kullback-Leibler Divergence', *IEEE Trans. Power Syst.*, 2018, **33**, (5), pp. 5147–5160
- [44] Gao, H., Liu J., Wang, L.: 'Robust coordinated optimization of active and reactive power in active distribution systems', *IEEE Trans. Smart Grid*, 2018, **9**, (5), pp. 4436–4447

7 Appendices

7.1 Lifting theorem

Let $\sigma \in \mathbb{R}^T$, and let $g(\cdot) : \mathbb{R}^R \rightarrow \mathbb{R}^T$ be a function with a \mathcal{K} -conic representable epigraph. The ambiguity set given by (28) can be lifted to (29). More details are provided in [32, 33].

$$\mathcal{P}' = \left\{ \mathbb{P} \in \mathcal{P}_0(\mathbb{R}^R) : \mathbb{E}_{\mathbb{P}'}[g(\tilde{\mathbf{w}}) \succeq_{\mathcal{K}} \sigma] \right\} \quad (28)$$

$$\mathcal{P} = \left\{ \mathbb{P} \in \mathcal{P}_0(\mathbb{R}^R \times \mathbb{R}^T) : \begin{array}{l} \mathbb{E}_{\mathbb{P}}[\tilde{\mathbf{u}}] = \sigma \\ \mathbb{P}[g(\tilde{\mathbf{w}}) \succeq_{\mathcal{K}} \tilde{\mathbf{u}}] = 1 \end{array} \right\} \quad (29)$$

7.2 Proof of equivalence between a general ambiguity set and a WKS-format ambiguity set

Using the general second-order ambiguity set (30) as an example, the following proof can prove the equivalence relationship between the general ambiguity set (30) and the WKS-format ambiguity set (25).

$$\mathcal{P}' = \left\{ \mathbb{P}' \in \mathcal{P}_0(\tilde{\mathbf{w}} \in \mathbb{R}^{|\mathcal{N}_s|}) : \begin{array}{l} \Omega' : \{\tilde{\mathbf{w}} \in [\mathbf{w}^{\min}, \mathbf{w}^{\max}]\} \\ \mathbb{P}'[\tilde{\mathbf{w}} \in \Omega'] = 1 \\ \mathbb{E}_{\mathbb{P}'}[\tilde{\mathbf{w}}] = \mu \\ \mathbb{E}_{\mathbb{P}'}[\tilde{\mathbf{w}}^2] \leq \sigma \end{array} \right\} \quad (30)$$

Proof: According to the definitions of \mathbf{C}_0 and \mathbf{f}_0 given by (25), the support set Ω' in (24) can be reformulated to a conic formulation as (31).

$$\left\{ \begin{array}{l} \Omega' = \{\tilde{\mathbf{w}} : \mathbf{w}^{\min} \leq \tilde{\mathbf{w}} \leq \mathbf{w}^{\max}\} \\ \Leftrightarrow \begin{bmatrix} \mathbf{E}_{|\mathcal{N}_s|} & -\mathbf{E}_{|\mathcal{N}_s|} \end{bmatrix} \tilde{\mathbf{w}} \leq \begin{bmatrix} \mathbf{w}^{\min} \\ -\mathbf{w}^{\max} \end{bmatrix} \end{array} \right. \quad (31)$$

The conic support set $\Omega' = \{\tilde{\mathbf{w}} : \mathbf{C}_0 \tilde{\mathbf{w}} \preceq_{\mathcal{K}_0} \mathbf{f}_0\}$ already satisfies the requirement of applying the *lifting theorem*; hence, \mathcal{P}' (30) can be lifted to \mathcal{P} (32).

$$\mathcal{P} = \left\{ \mathbb{P} \in \mathcal{P}_0(\begin{array}{c} \tilde{\mathbf{w}} \in \mathbb{R}^{|\mathcal{N}_s|} \\ \tilde{\mathbf{u}} \in \mathbb{R}^{|\mathcal{N}_s|} \end{array}) : \begin{array}{l} \Omega = \left\{ \tilde{\mathbf{w}} : \begin{array}{l} \mathbf{C}_0 \tilde{\mathbf{w}} \preceq_{\mathcal{K}_0} \mathbf{f}_0 \\ \tilde{\mathbf{w}}^2 \leq \tilde{\mathbf{u}} \end{array} \right\} \\ \mathbb{P}[(\tilde{\mathbf{w}}, \tilde{\mathbf{u}}) \in \Omega] = 1 \\ \mathbb{E}_{\mathbb{P}}[\tilde{\mathbf{w}}] = \mu \\ \mathbb{E}_{\mathbb{P}}[\tilde{\mathbf{u}}] = \sigma \end{array} \right\} \quad (32)$$

In the lifted \mathcal{P} (32), the new auxiliary vector $\tilde{\mathbf{u}}$ introduces the second-order information into the inequality $\tilde{\mathbf{w}}^2 \leq \tilde{\mathbf{u}}$ of Ω . The inequality can be converted to a second-order conic formulation, as given by (33).

$$\left\{ \begin{array}{l} \tilde{\mathbf{w}}^2 \leq \tilde{\mathbf{u}} \\ \Leftrightarrow \tilde{w}_s^2 \leq \tilde{u}_s = [(\tilde{u}_s + 1)/2]^2 - [(\tilde{u}_s - 1)/2]^2 \\ \Leftrightarrow \tilde{w}_s^2 + [(\tilde{u}_s - 1)/2]^2 \leq [(\tilde{u}_s + 1)/2]^2 \\ \Leftrightarrow \left\| \begin{bmatrix} \tilde{w}_s \\ (\tilde{u}_s - 1)/2 \end{bmatrix} \right\|_2 \leq (\tilde{u}_s + 1)/2 \\ \Leftrightarrow \left[\begin{array}{c} \tilde{w}_s \\ (\tilde{u}_s - 1)/2 \\ (\tilde{u}_s + 1)/2 \end{array} \right] \in \mathbb{L}^3, \forall s \in \mathcal{N}_s \end{array} \right. \quad (33)$$

Based on the definitions of \mathbf{C}_s , \mathbf{D}_s , \mathbf{f}_s , and \mathcal{K}_s in (25), the second-order conic formulation in (33) can be unified into the conic formulation given by (34).

$$\left\{ \begin{array}{l} \left[\begin{array}{c} \tilde{w}_s \\ (\tilde{u}_s - 1)/2 \\ (\tilde{u}_s + 1)/2 \end{array} \right] = \left[\begin{array}{cccccc} 0 & \cdots & 0 & \underbrace{1}_{s^{th}} & 0 & \cdots & 0 \\ 0 & \cdots & 0 & 0 & 0 & \cdots & 0 \\ 0 & \cdots & 0 & 0 & 0 & \cdots & 0 \end{array} \right] \tilde{\mathbf{w}} + \\ \left[\begin{array}{ccccc} & \underbrace{s^{th}}_{0} & & & \\ 0 & \cdots & 0 & 0 & \cdots & 0 \\ 0 & \cdots & 0 & 1/2 & 0 & \cdots & 0 \\ 0 & \cdots & 0 & 1/2 & 0 & \cdots & 0 \end{array} \right] \tilde{\mathbf{u}} - \left[\begin{array}{c} 0 \\ 1/2 \\ -(1/2) \end{array} \right] \\ \Leftrightarrow C_s \tilde{\mathbf{w}} + D_s \tilde{\mathbf{u}} \preceq_{\mathcal{K}_s} f_s, \forall s \in \mathcal{N}_s \end{array} \right. \quad (34)$$

Based on the definitions of \mathbf{A} , \mathbf{B} , and \mathbf{e} in (25), the expectation terms of (32) can be rewritten as (35).

$$\begin{cases} \mathbb{E}_{\mathbb{P}}[\tilde{\mathbf{w}}] = \mu \\ \mathbb{E}_{\mathbb{P}}[\tilde{\mathbf{u}}] = \sigma \end{cases} \Leftrightarrow \mathbb{E}_{\mathbb{P}}[\mathbf{A}\tilde{\mathbf{w}} + \mathbf{B}\tilde{\mathbf{u}}] = \mathbf{e} \quad (35)$$

According to (31) to (35), general ambiguity set \mathcal{P}' (30) can be equivalently converted into WKS-format ambiguity set \mathcal{P} (25). The proof is completed. \square

7.3 System parameters

The partial details of the parameter settings are listed in Table 5, which are similar to the settings used in [14]. Additionally, any other parameter settings without special declaration, such as the initial unit output, and load data are configured as IEEE standard data.

Table 5 Partial details of the experimental parameters.

Parameter	Setting
c_{dj}^w	50 \$/MWh
c_{dq}^l	500 \$/MWh
c_{di}^g	350 \$/MWh
R_i^{up}	40% of maximal output of generator i
R_i^{dn}	40% of maximal output of generator i
r_i^{up}	40% of maximal output of generator i
r_i^{dn}	40% of maximal output of generator i
Buses of WPGs	#12, #17, #49, #59, #70, #77, #92, #100

7.4 Details of cases

The details of the four cases employed for the experiments are shown in Fig. 8. The maximal, rated, and minimal generation of these WPGs are 300 MW, 100 MW, and 0 MW. Therefore, 100 MW is selected as a threshold. If the generation of WPGs is higher than 100 MW, the generation is regarded as sufficient; otherwise, it is insufficient. According to [44], typical cases include case 1 (sufficient wind power) and case 2 (insufficient wind power). In addition to cases 1 and 2, this paper adds case 3 (wind power decreases from sufficient to insufficient over time) and case 4 (wind power increases from insufficient to sufficient over time). As a result, the four cases can represent the most typical cases of WPG operation.

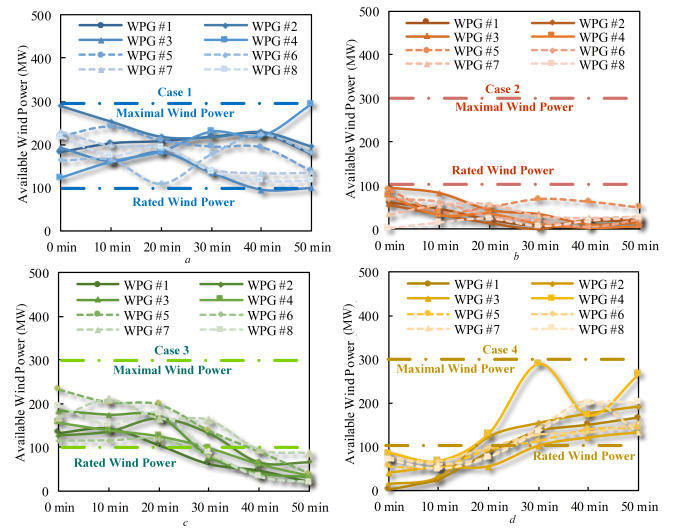


Fig. 8: Curves of available wind power generation in the four cases.

7.5 Formulation of A-SLED

The compact formulation of A-SLED is shown by (36).

$$\left\{ \begin{array}{l} \min_{\mathbf{p}} \left\{ c(\mathbf{p}) + \max_{\tilde{\mathbf{w}}} \min_{\mathbf{y}} (\mathbf{d}^\top \mathbf{y}) \right\} \\ \text{s.t. } H_{LED}(\mathbf{p}) = 0, \\ G_{LED}(\mathbf{p}) \leq 0, \\ H_{RED}(\mathbf{p}, \tilde{\mathbf{w}}, \mathbf{y}, \Gamma) = 0, \\ G_{RED}(\mathbf{p}, \tilde{\mathbf{w}}, \mathbf{y}, \Gamma) \leq 0. \end{array} \right. \quad (36)$$

In (36), $H_{LED}(\cdot) = 0$ and $H_{RED}(\cdot) = 0$ represent the equality constraints in LED and RED stages; $G_{LED}(\cdot) \leq 0$ and $G_{RED}(\cdot) \leq 0$ denote the inequality constraints in LED and RED stages; Γ is the budget parameter that determined the pessimistic degree of the worst-case scenario in an uncertainty set.

According to [42], the uncertainty set characterizing the uncertain wind power generation is expressed by (37).

$$\tilde{\mathbf{w}} \in [\mathbf{w}^{min}, \mathbf{w}^{max}] \quad (37)$$

In order to adjust the pessimistic degree of the worst-case scenario in the uncertainty set, adjustable robust constraint (38) is introduced to restrict the number of the worst-case realizations.

$$\sum_{s=1}^{|\mathcal{N}_s|} \left[\frac{\tilde{w}_s - \mu_s}{w_s^+} \cdot \rho_s^+ + \frac{\mu_s - \tilde{w}_s}{w_s^-} \cdot \rho_s^- \right] \leq \Gamma \quad (38)$$

In (38), μ_s is the wind power prediction, which is the first-order information; w_s^+ and w_s^- are the upward and downward fluctuation ranges; ρ_s^+ and ρ_s^- are 0-1 integer variables.

Based on the construction of (38), if $\mu_s \leq \tilde{w}_s$, then $\rho_s^+ = 1$ and $\rho_s^- = 0$; otherwise, $\rho_s^+ = 0$ and $\rho_s^- = 1$. Γ denotes the number of times that the wind power generation reaches the boundary values. Therefore, the conservativeness of the strategy can be adjusted by tuning the value of Γ . A larger Γ leads to a more conservative optimization. In this regard, ARO is equivalent to traditional robust optimisation when Γ is set to its maximum. For models with 30-min resolutions, the range of Γ is $[0, 16]$. Therefore, budgets $\Gamma = 6$, $\Gamma = 10$, and $\Gamma = 14$ that represent different levels of robustness are selected for the comparison.

To solve A-SLED, this study follows the method described in [42], which employs a column-constraint generation algorithm, the Big-M method, and the duality theorem. For more details regarding the solution method, please refer to [42].